Journal of Alloys and Compounds 509 (2011) 4660–4669

Contents lists available at ScienceDirect

Journal of Alloys and Compounds

journal homepage: www.elsevier.com/locate/jallcom

^{119}Sn Mössbauer spectroscopy study of the magnetic properties of the $HfFe_6Ge_6$-type compounds: $SmMn_6Sn_4Ge_2$ and $GdMn_6Sn_4Ge_2$

G. Venturini*, P. Lemoine, B. Malaman

Institut Jean Lamour, CNRS (UMR 7198) – Nancy Université, B.P. 70239, 54506 Vandoeuvre-les-Nancy Cedex, France

ARTICLE INFO

Article history:
Received 5 November 2010
Received in revised form 25 January 2011
Accepted 28 January 2011
Available online 4 February 2011

Keywords:
Rare-earth alloys and compounds
Transition metal alloys and compounds
Single crystal
^{119}Sn Mössbauer spectroscopy

ABSTRACT

The $HfFe_6Ge_6$-type compound $SmMn_6Sn_4Ge_2$ has been studied by single-crystal magnetisation and ^{119}Sn Mössbauer spectroscopy. The compound orders ferromagnetically at T_c = 420 K and displays an easy-axis anisotropy from T_c to T_{SR} = 130 K. Below T_{SR}, both magnetisation and ^{119}Sn Mössbauer spectroscopy measurements indicate a deviation from the [0 0 1] direction and the presence of easy-cone anisotropy. The angle of the moments with respect to the [0 0 1] direction is estimated to 26–31° from Mössbauer spectroscopy results, in good accordance with the magnetisation results. The isotypic compounds $GdMn_6Sn_4Ge_2$ and $GdMn_6Sn_6$ studied by ^{119}Sn Mössbauer spectroscopy display easy plane anisotropy in the whole temperature range 300–4.2 K. The anisotropy behaviours of the $LMn_6Sn_4Ge_2$ compounds are discussed and the coexistence of easy cone anisotropy for both the $SmMn_6Sn_4Ge_2$ and $HoMn_6Sn_4Ge_2$ suggests the play of a positive second-order anisotropy constant of the Mn sublattice.

1. Introduction

The crystallographic and magnetic properties of $HfFe_6Ge_6$-type $LMn_6Sn_4Ge_2$ compounds (L = Sc, Y, lanthanides) have been reported in a previous paper [1]. It has been observed that the replacement of tin by germanium enables the stabilisation of the simple hexagonal structure even for the light rare earths compounds which usually crystallize in more complicated orthorhombic structures [2]. The thermomagnetic curves have shown that the compound $SmMn_6Sn_4Ge_2$ was characterized by a ferromagnetic-like behaviour and displayed a second magnetic transition at low temperature. Moreover, the isotherm curves display a hysteresis cycle at room temperature, a feature never observed at room temperature for LMn_6X_6 compounds (X = Sn, Ge). The neutron diffraction study of $TbMn_6Sn_4Ge_2$ compound has evidenced a ferrimagnetic structure with a easy plane anisotropy at low temperature contrary to the $TbMn_6Sn_6$ compound characterized by a strong easy axis anisotropy [3,4]. The compound $TmMn_6Sn_4Ge_2$, studied by neutron diffraction and Mössbauer spectroscopy, displays a more complicated behaviour characterized by an easy plane helimagnetic structure at room temperature and an easy axis ferrimagnetic structure at low temperature [5]. The Mössbauer study has provided interesting information on the intermediate temperature range characterized by the tilting of the helical plane. The relative behaviour of the magnetocrystalline anisotropy of the Tb and Tm compounds suggests that the easy magnetisation direction is driven by the second order CEF parameter and that the easy axis magnetisation of the L moment is related to a corresponding positive α_j Steven's coefficient. This seems to be consistent with the rather hard magnetic behaviour of $SmMn_6Sn_4Ge_2$. In order to check this assumption, we have decided to investigate the magnetic properties of $SmMn_6Sn_4Ge_2$ with single crystal magnetisation measurements and ^{119}Sn Mössbauer spectroscopy. This study led us to also undertake Mössbauer spectroscopy investigations of the isotypic compounds $GdMn_6Sn_4Ge_2$ and $GdMn_6Sn_6$.

2. Experimental methods

The polycrystalline samples have been prepared starting from the ternary compounds LMn_6Sn_6 and LMn_6Ge_6 (L = Sm, Gd) previously prepared in an induction furnace. The stoichiometric amounts of LMn_6Sn_6 and LMn_6Ge_6 are finely ground, compacted into pellets and sealed in silica tube under argon (0.1 atm). The silica tubes are then annealed at 873 K during one month. The samples have been checked by conventional X-ray powder analysis (Guinier Co Kα and XPERT Pro Cu Kα) and the crystal structures have been refined using the Fullprof software [6].

The $SmMn_6Sn_4Ge_2$ single crystals have been obtained starting from a mixture of the ternary compounds and tin with the overall composition $SmMn_6Sn_{49}Ge_1$. The mixture is put into a silica tube with a quartz-wool stopper. The silica tube is sealed under argon (267 mbar) and heated to 1073 K (at 50 K/h) for 24 h. Then it is cooled down to 1023 K (6 K/h), heated again up to 1063 K at the same rate and finally slowly cooled down to 773 K in 65 h. The tube is quickly removed from the furnace, inverted and centrifuged manually using a David's sling device. The Sn flux lies at the bottom of the tube and the crystals remain on the quartz-wool stopper.

The magnetisation measurements have been performed on a MANICS DSM8 magneto-susceptometer in the temperature range 4.2–500 K and in fields up to 1.5 T.

The ^{119}Sn Mössbauer measurements were carried out using a constant-acceleration spectrometer in standard transmission geometry. Several spectra were recorded between 300 and 4.2 K in a liquid helium cryostat. The velocity scale was

* Corresponding author. Tel.: +33 3 83 68 46 73; fax: +33 3 83 68 46 11.
E-mail address: Gerard.Venturini@lcsm.uhp-nancy.fr (G. Venturini).

0925-8388/$ – see front matter © 2011 Elsevier B.V. All rights reserved.
doi:10.1016/j.jallcom.2011.01.201

Table 1
Refined cell parameters, atomic coordinates and occupation factors (m_j) of $GdMn_6Sn_{\approx 4}Ge_{\approx 2}$ and $SmMn_6Sn_{\approx 4}Ge_{\approx 2}$.

	$GdMn_6Sn_{\approx 4}Ge_{\approx 2}$	$SmMn_6Sn_{\approx 4}Ge_{\approx 2}$
a (Å)	5.4269(1)	5.4436(1)
c (Å)	8.7582(2)	8.7766(2)
z_{Mn}	0.2343(3)	0.2352(3)
z_{Sn3}	0.3359(2)	0.3359(2)
$m_{Sn(2c)}$ [$m_{Ge(2c)}$]	0.071(7) [0.929(7)]	0.031(7) [0.969(7)]
$m_{Sn(2d)}$ [$m_{Ge(2d)}$]	0.810(8) [0.190(8)]	0.817(9) [0.183(9)]
r_{Bragg}, r_f, χ^2	7.61, 6.64, 41.5	8.35, 6.80, 37.7

calibrated with a ^{57}CoRh source (25 mCi) and a metallic iron foil at room temperature. We used a $Ba^{119m}SnO_3$ source (10 mCi) kept at room temperature which also served as the reference for the isomer shifts. A polycrystalline absorber with natural abundance of ^{119}Sn isotope and thickness of $\sim 15\,mg\,cm^{-2}$ was used. A palladium foil of 0.5 mm thickness was used as a critical absorber for tin X-rays. The Mössbauer spectra were fitted with a least-squares method program assuming Lorentzian peaks [7].

3. Crystallographic data

The cell parameters, atomic coordinates and the X site occupancy factors (m_j) have been refined. The results are gathered in Table 1. They show that the germanium atoms are mainly located in the 2(c) site, within the Mn–(L,X)–Mn slab (Fig. 1), as previously observed [1]. However, the refinements indicate that a small quantity of germanium atoms also occupies the 2(d) site, within the Mn–X–X–X–Mn slab, while some tin atoms remain in the 2(c) site. We will see hereafter that the distribution of the hyperfine parameters also accounts for these non-fully occupied sites. There is also a significant variation of the z_{Mn} coordinate with respect to that measured in pure ternary compounds LMn_6Sn_6 [8]. This variation accounts for a relative displacement of the Mn atoms towards the Ge plane in good accordance with the smaller size of the Ge atom. This variation also yields a shortening of the L-Mn distances with respect to the corresponding distance in the ternary stannide, a feature which should be related to electronic structure calculations in LT_6X_6 compounds [9]. According to this study, there is a significant hybridization between the L and T states and it is suggested that the preferential occupation of the 2(c) site by the germanium atoms and the correlative shortening of the L-Mn distances within the Mn–(L,X)–Mn slab, probably originate from this effect.

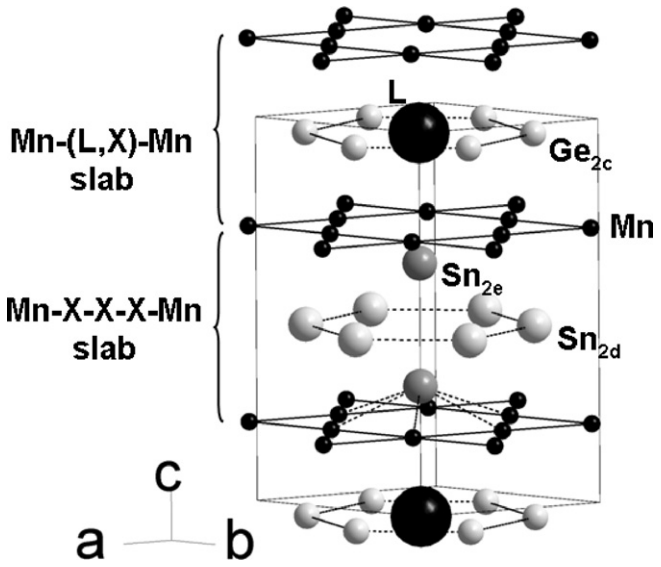

Fig. 1. Representation of the structure of $LMn_6Sn_4Ge_2$ compounds (L = Gd, Sm).

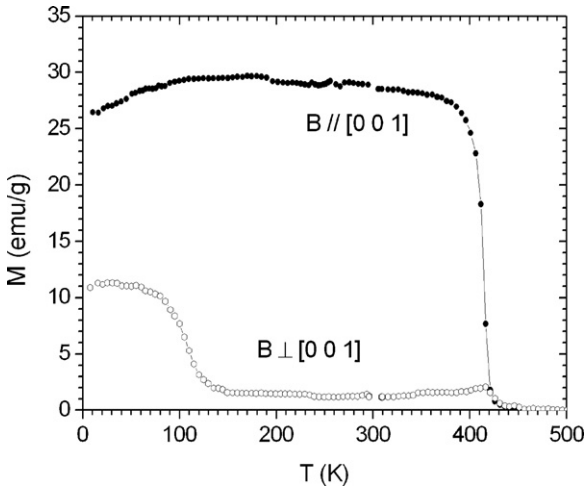

Fig. 2. Thermal variation of the magnetisation of a $SmMn_6Sn_4Ge_2$ single-crystal with the field (B_{appl} = 0.05 T) applied, respectively, along and perpendicular to the [0 0 1] direction.

4. Magnetisation study of a $SmMn_6Sn_4Ge_2$ single crystal

A small well-shaped single crystal weighting 4.9 mg has been isolated from the melt and studied by magnetisation measurements. Fig. 2 displays the thermal variation of the magnetisation measured with the field (B = 0.05 T) applied along the hexagonal axis and perpendicular to it. Below the Curie point (T_C = 420 K), the magnetisation measured along the hexagonal axis is always large and only displays a slight reduction at low temperature (T < 100 K). On the contrary, the magnetisation with the field perpendicular to the c axis is very weak in the high temperature range and only becomes significant below 130 K. This behaviour indicates that, below the Curie point and down to 130 K, the easy magnetisation axis is parallel to the hexagonal axis. The low temperature behaviour suggests that the easy axis leaves the [0 0 1] direction but without reaching the (0 0 1) plane. This assumption is confirmed by the isotherm curves recorded at 300 and 4.2 K (Fig. 3). At 300 K, there is no spontaneous magnetisation in the direction perpendicular to the c axis while the magnetisation well saturates along the c axis. At 4.2 K, there is spontaneous magnetisation along and perpendicular to the [0 0 1] direction thus accounting for an easy direction intermediate between the c axis and the (0 0 1) plane. In order to get information on the magnitude of the deviation angle, a magnetisation of the "free" crystal has been also done leading to a maximum magnetisation value $M = 12.6\mu_B$/mole (Fig. 3). This value has been used to calculate the angle α from the magnetisations measured along [0 0 1] and perpendicular to it (Fig. 4). It shows that, in the range where almost saturated values are reached, the angle α is close to 27–30°. When the field is applied along [0 0 1], it closes the angle α down to 26° and when it is applied perpendicular to [0 0 1], it opens the angle α up to 32°. It seems that the angle varies more easily when the applied field is perpendicular to [0 0 1], a feature which may be related to a more efficient gain in Zeeman energy in this configuration.

5. ^{119}Sn Mössbauer spectroscopy

The initial aim of this study was to check the magnetic behaviour of $SmMn_6Sn_4Ge_2$. Since its magnetic structures cannot be determinate from a neutron diffraction study (*too high absorption cross section of samarium nucleus i.e.* 42,000 barns *at* λ = 2 Å), a ^{119}Sn Mossbauer study was undergo. According to the obtained results, we have decided to examine the hyperfine parameters of the corresponding compound $GdMn_6Sn_4Ge_2$ also characterized by highly

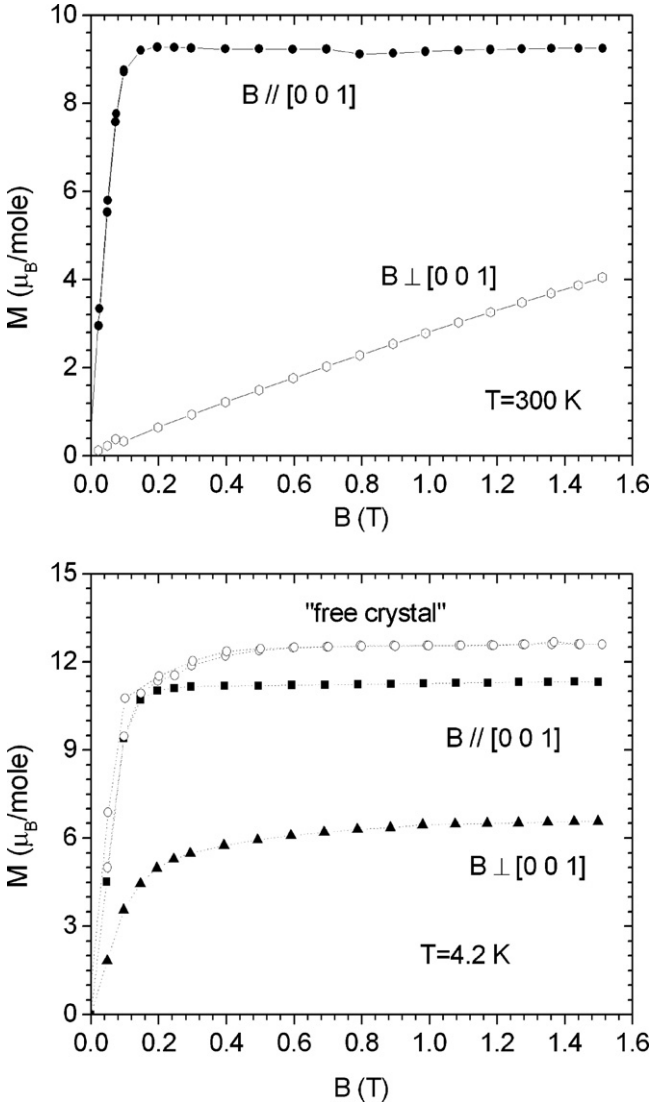

Fig. 3. Magnetisation vs. field of a $SmMn_6Sn_4Ge_2$ single crystal with the field applied along and perpendicular to the direction [0 0 1]. (*The 4.2 K plot also shows the magnetisation of the crystal free to rotate in the field.*)

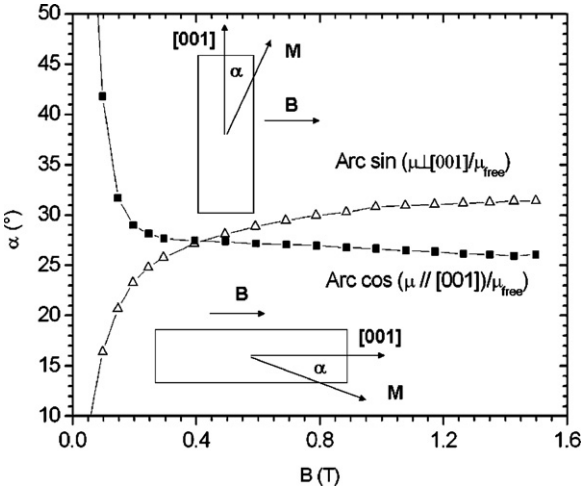

Fig. 4. Calculated angle α between the moment direction and the c axis in the two configurations (*i.e. B applied along and perpendicular to the direction* [0 0 1]).

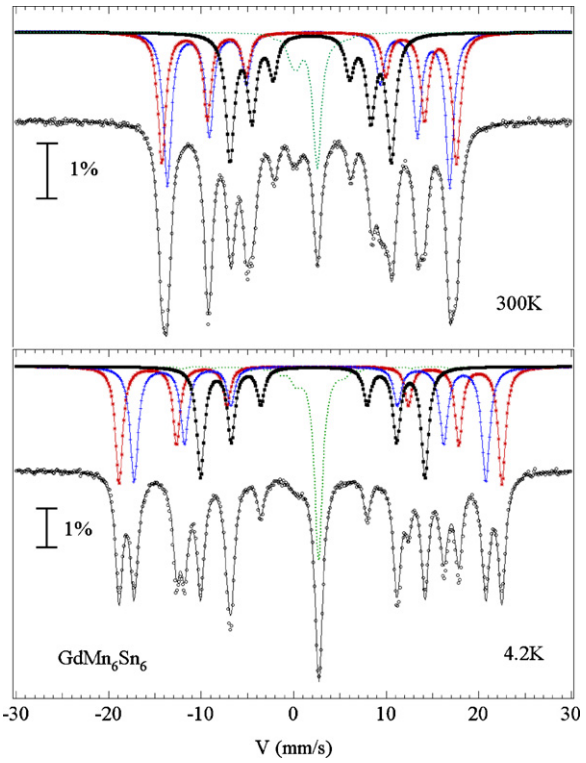

Fig. 5. Observed and calculated ^{119}Sn Mössbauer spectra of $GdMn_6Sn_6$ at 300 and 4.2 K (the dotted line represents the impurities contribution).

absorbing nucleus (*Gd*: 260,000 barns *at* $\lambda = 2$ Å). At this step, the hyperfine parameters of $GdMn_6Sn_4Ge_2$ were found inconsistent with those reported for isotypic $GdMn_6Sn_6$ [10] and we therefore decided to also perform Mössbauer spectroscopy on this parent compound. The fitting procedure has been largely described in [11]. According to their rank in complexity, we will present the results in the inverse order.[1]

5.1. $GdMn_6Sn_6$

The 4.2 K spectrum is characterized by fifteen rather well separated peaks accounting for the three crystallographic sites of the $HfFe_6Ge_6$-type $GdMn_6Sn_6$ structure (Fig. 5). The overall aspect of the spectrum well agrees with that reported by Amako et al. [10]. The positions of the peaks enable a good estimation of the initial hyperfine parameters used for the refinements. The three tin sites are located in highly symmetric positions: *6mm* for the 2(e) site and *−6m2* for 2(c) and 2(d) sites. In all cases, the V_{zz} principal axis of the EFG tensor should be parallel to [0 0 1] and the asymmetry parameter $\eta = 0$. For the three sextets, the large hyperfine field values imply to consider the quadrupole interaction as a perturbation of the magnetic hyperfine interaction. For each site, we have refined the relative area, linewidth (Γ), isomer shift (IS), quadrupole splitting (QS) and hyperfine field (B_{hf}).

The studied sample contains $MnSn_2$, $GdMn_xSn_2$ and tin as impurities. At low temperature, only the magnetic compound $MnSn_2$, whose hyperfine parameters are well known [12], and tin have been taken into account in the fits. Their relative areas are refined to 2 and 11%, respectively. At room temperature, only the paramagnetic $GdMn_xSn_2$ compound (2%) and tin (7%) are clearly observed and have been refined (see Fig. 5).

[1] *Remark*: For simplicity, in the following, we will use the terms "field" or "hyperfine field" in spite of the more correct term "transferred hyperfine field on tin nuclei".

Table 2
Hyperfine parameters of $GdMn_6Sn_6$ at 300 K (χ^2 = 3.64) and 4.2 K (χ^2 = 8.14).

T (K)	Sites	Area (%) ±0.03	Γ (mm/s) ±0.06	IS (mm/s) ±0.08	QS (mm/s) ±0.08	B (T) ±0.3
300	2(e)	0.29	1.10	2.06	−0.07	12.6
	2(d)	0.28	1.01	2.12	−0.73	23.1
	2(c)	0.33	1.01	1.95	−0.52	22.1
4.2	2(e)	0.32	0.97	2.12	−0.13	17.7
	2(d)	0.33	0.94	2.20	−0.77	30.2
	2(c)	0.35	1.03	1.98	−0.46	27.8

The results of the refinements are gathered in Table 2. The relatively high χ^2 value obtained for the sample recorded at 4.2 K seems to be connected with texture effects since the intensities of the second and fifth Mössbauer lines are systematically reduced (see Fig. 5). Except for the hyperfine fields which significantly increase upon cooling, the refined hyperfine parameters do not greatly vary. The 4.2 K values of the hyperfine field are close to the values refined at 80 K by Amako et al. [10]. The absolute value of the quadrupole splitting also well agrees with the reported data [10] but the isomer shifts are rather different. The values of the QS are negative and close to those refined for $YMn_6Sn_{5.42}In_{0.58}$ pseudo-single crystal for which the orientation of the moments are known to be perpendicular to [0 0 1] [13]. Therefore, the hyperfine parameters measured for $GdMn_6Sn_6$ are in good agreement with the results of a "hot neutron" diffraction study [14].

5.2. $GdMn_6Sn_4Ge_2$

According to the crystal structure refinement (Section 3.), the $HfFe_6Ge_6$-type $GdMn_6Sn_4Ge_2$ compound is characterized by two sites 2(e) and 2(d) with a large occupation by tin atoms and one site 2(c) mainly occupied by germanium atoms. This feature agrees with the corresponding spectra characterized by a less number of intense peaks (Fig. 6). Moreover, there are additional weak absorption peaks and several shoulders on the intense peaks. We guess that these features may arise from additional sub-sites depending on their local environment and we have performed the refinements taking into account these possible sub-sites which are defined in the following section.

5.2.1. Sub-sites definitions

The estimation of the possible sub-sites with significant intensity has been done considering the binomial distribution:

$$P_p = C_p^n . x^p . (1-x)^{n-p} \quad (1)$$

where P_p is the population for the considered case, n is the number of Sn and Ge neighbours for a given site, p is the number of Ge neighbours and x the concentration of Ge on the considered site.

The tin atoms in site 2(d) are located in a Mn_6 trigonal prism (Fig. 7). The two triangular faces of the prism are capped by a Ge(Sn) atom in 2(c) position and there are three Sn(Ge) 2(d) neighbours in the equatorial plane. This gives rise to the possible sub-sites distribution given in columns 2 and 3 of Table 3. For this site, we will only consider the distribution of Ge(2d) atoms around Sn(2d) nucleus. We guess that an increasing number of Ge neighbours will lead to a tightening of the Mn planes around the Sn(2d) site and, in turn, a contraction of the Mn–Sn(2d) distances. Such a variation of the interatomic distances should yield a change of the involved hyperfine field.

The same applies for the remaining tin atoms in site 2(c). However in this case, we will only consider the distribution of the Ge(2d) atoms around the Sn(2c) nucleus (Table 3). In this case, we guess that a Ge(2d) atom will attract the Mn_3 triangular face yielding an increase of the Mn–Sn(2c) distances. This should also yield a change of the hyperfine field on the Sn(2c) nucleus.

The Sn(2e) atom is surrounded by an hexagon made of six Sn(Ge) atoms in 2(d) position. The corresponding distribution is given in column 6 of Table 3. We have neglected the possible different distributions of the Ge and Sn atoms on the corners of the hexagon. There are four significant distributions. We guess that the replacement of tin by germanium in the 2(d) position will shrink the Mn plane towards the Sn(2e) nucleus yielding variations of the Mn–Sn(2e) distances.

All these hypotheses will be nicely improve by the refinements of the spectra.

5.2.2. Refinements of the hyperfine parameters

According to previous section, the refinements have been undertaken considering nine tin sub-sites: four for the 2(e) position, three for the 2(d) position and two for the 2(c) position. In order to minimize the number of free parameters, for each crystallographic position, the linewidths (Γ) of the corresponding sub-sites have been constrained to be equal. Although the peaks were strongly convoluted, we expected that the refined area of each sub-site enabled a significant site attribution. The refined parameters are given in Table 4. The estimated relative areas of the tin and $MnSn_2$

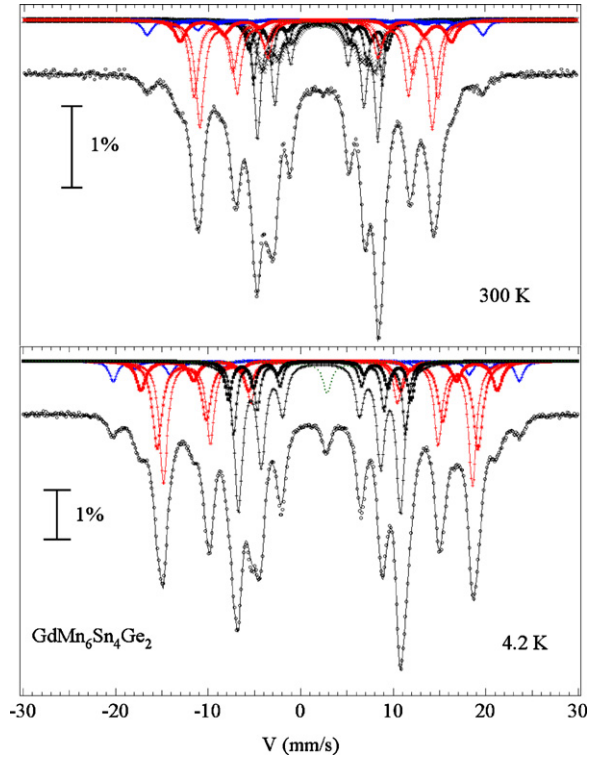

Fig. 6. Observed and calculated ^{119}Sn Mössbauer spectra of $GdMn_6Sn_4Ge_2$ at 300 and 4.2 K (the dotted line represents the impurities contribution).

Table 3
Distribution of site populations in the case of $GdMn_6Sn_{\approx 4}Ge_{\approx 2}$ compound (bold characters correspond to the considered distributions).

Number of Ge	2(d) site occupied by 0.19 Ge and 0.81 Sn		2(c) site occupied by 0.93 Ge and 0.07 Sn		2(e) site occupied by 0.00 Ge and 1.00 Sn
	3× 2(d) Neighbours	2× 2(c) Neighbours	3× 2(c) Neighbours	2× 2(d) Neighbours	6× 2(d) Neighbours
0 Ge	**0.531**	0.005	<0.001	**0.656**	**0.282**
1 Ge	**0.374**	0.130	0.014	**0.308**	**0.397**
2 Ge	**0.088**	0.865	0.182	0.036	**0.233**
3 Ge	0.007	–	0.804	–	**0.073**
4 Ge	–	–	–	–	0.013
5 Ge	–	–	–	–	0.001
6 Ge	–	–	–	–	<0.001

impurities are 1.6 and 0.8%, respectively. The QS and IS values of the different sub-sites are rather homogeneous and close to those refined for $GdMn_6Sn_6$. Particularly, the sign (<0) and magnitude of the QS values indicate that the direction of the hyperfine field is perpendicular to V_{zz} as observed for $GdMn_6Sn_6$ and therefore indicate that the moment direction lies in the (0 0 1) plane in both compounds.

The refined areas of the different sub-sites rather well fit the theoretical distribution given in Table 3 and enable us to relate the hyperfine field of the different sub-sites to the number of Ge neighbours. The evolution of the hyperfine field as a function of the number of Ge neighbours is given in Fig. 8. The 2(c) sub-sites are characterized by a negative slope and the 2(e) and 2(d) sub-sites by a positive slope. This should be attributed to the relative position of the Ge neighbours. For the 2(e) and 2(d) sites the Ge neighbours are located in the same Mn–X–X–X–Mn slab and their presence tightens the Mn planes around the Sn nuclei. For the 2(c) site, in the Mn–(L,X)–Mn slab, the involved Ge neighbour lies in the adjacent Mn–X–X–X–Mn slabs and its presence dilates the Mn planes around the Sn nuclei. This means that the increase of the field is correlated to the decrease of the Mn–Sn distance.

5.3. $SmMn_6Sn_4Ge_2$

The spectra of $SmMn_6Sn_4Ge_2$ display some resemblance with the spectra of $GdMn_6Sn_4Ge_2$ in fair accordance with similar crystallographic properties (Fig. 9). However, the relative positions of the absorption peaks clearly indicate a change of the sign of the quadrupole splitting which should be related to the different magnetic properties observed by magnetisation measurements. In addition, the internal peaks related to the 2(e) sub-sites are less split thus indicating smaller corresponding hyperfine fields.

The hyperfine parameters have been refined in the same way and the results are gathered in Table 5. The estimated relative areas of the tin and $MnSn_2$ impurities are 2.0 and 1.2% respectively. At 300 K, owing to the weak splitting of the internal 2(e) sites, only the two mostly populated sub-sites have been considered. The corresponding refinements converge to $\chi^2 = 2.96$ with rather fair linewidth of the absorption peaks.

As suggested above, the fields measured for the 2(e) sub-sites are significantly smaller than those measured for the compound $GdMn_6Sn_4Ge_2$ and the values of the quadrupole splitting are positive. The different QS values refined for the 4.2 and 300 K spectra should be related to the re-orientation of the moments observed by magnetisation measurements. In order to check this phenomenon, several spectra have been recorded at various temperatures (Fig. 10). The thermal variation of the refined QS values, displayed in Fig. 11a, clearly indicates an almost constant value in the range 160–300 K and a sudden change around 130 K in fair accordance with the results of thermomagnetic data. In the magnetic state, the apparent quadrupole splitting is expressed, in the

Table 4
Hyperfine parameters of $GdMn_6Sn_{\approx 4}Ge_{\approx 2}$ at 300 K ($\chi^2 = 4.46$) and 4.2 K ($\chi^2 = 3.09$).

T (K)	Sites	Area (%) ±0.03	Γ (mm/s) ±0.06	IS (mm/s) ±0.08	QS (mm/s) ±0.08	B (T) ±0.3
300	0/6 Ge	0.11	0.91	1.96	−0.13	9.1
	1/6 Ge	0.22	0.91	1.94	−0.17	9.6
	2/6 Ge	0.12	0.91	1.94	−0.14	10.3
	3/6 Ge	0.04	0.91	1.97	−0.22	11.1
	2(e)	0.49				
	0 Ge	0.28	1.15	2.04	−0.72	18.5
	1/3 Ge	0.13	1.15	2.07	−0.79	19.6
	2/3 Ge	0.04	1.15	2.14	−0.92	21.7
	2(d)	0.45				
	0 Ge	0.03	1.21	1.83	−0.61	26.7
	1/2 Ge	0.01	1.21	1.83	−0.61	22.4
	2(c)	0.04				
4.2	0/6 Ge	0.03	0.88	2.30	−0.05	11.6
	1/6 Ge	0.20	0.88	2.11	−0.17	12.7
	2/6 Ge	0.15	0.88	2.10	−0.14	13.5
	3/6 Ge	0.07	0.88	2.12	−0.13	14.4
	2(e)	0.45				
	0 Ge	0.27	1.12	2.20	−0.69	24.5
	1/3 Ge	0.14	1.12	2.18	−0.73	25.4
	2/3 Ge	0.06	1.12	2.18	−0.66	28.3
	2(d)	0.47				
	0	0.04	1.16	1.89	−0.41	32.1
	1/2	0.02	1.16	1.89	−0.41	26.9
	2(c)	0.05				

Table 5
Hyperfine parameters of $SmMn_6Sn_{\approx 4}Ge_{\approx 2}$ at 300 K ($\chi^2 = 2.96$) and 4.2 K ($\chi^2 = 4.17$).

T (K)	Sites	Area (%) ±0.03	Γ (mm/s) ±0.06	IS (mm/s) ±0.08	QS (mm/s) ±0.08	B (T) ±0.3
300	0/6 Ge	–	–	–	–	–
	1/6 Ge	0.27	1.04	2.06	0.35	4.8
	2/6 Ge	0.20	1.13	2.06	0.32	5.5
	3/6 Ge	–	–	–	–	–
	2(e)	0.47				
	0/3 Ge	0.24	1.07	2.15	1.44	19.3
	1/3 Ge	0.15	0.99	2.14	1.48	20.2
	2/3 Ge	0.07	1.34	2.15	1.54	22.8
	2(d)	0.46				
	0/2 Ge	0.05	1.34	2.15	0.89	26.6
	1/2 Ge	0.04	1.07	2.17	1.26	21.8
	2(c)	0.09				
4.2	0/6 Ge	0.03	1.11	1.48	0.23	7.6
	1/6 Ge	0.22	1.11	2.10	0.10	9.1
	2/6 Ge	0.17	1.11	2.12	0.08	9.9
	3/6 Ge	0.02	1.11	2.61	0.03	11.4
	2(e)	0.44				
	0 Ge	0.26	1.21	2.19	1.09	25.9
	1/3 Ge	0.16	1.21	2.18	1.15	27.0
	2/3 Ge	0.05	1.21	2.27	1.13	29.9
	2(d)	0.47				
	0	0.04	1.38	1.84	1.00	33.4
	1/2	0.02	1.38	1.84	1.00	27.4
	2(c)	0.06				

case of zero asymmetry parameter ($\eta = 0$), as:

$$QS = \tfrac{1}{2}\, eQV_{zz}\,(3\ \cos^2\theta - 1) \qquad (2)$$

where Q is the quadrupole moment, V_{zz} the EFG tensor element and θ the angle between the hyperfine field B_{hf} and the EFG principal axis.

At 160 K, the magnetisation measured on the single crystal indicates that the moments are aligned along the c axis i.e. $\theta = 0°$. Assuming that the term $1/2\ eQV_{zz}$ does not greatly vary upon cooling, the measured QS values allow an estimation of the angle θ variation below 130 K. The results, displayed in Fig. 11b, indicate a rather weak re-orientation of the Sn_{2d} hyperfine field and a larger reorientation of Sn_{2e} hyperfine field. This apparent discrepancy should be related to the play of an anisotropic field transfer. The occurrence of anisotropic transfer has been clearly observed on a $YMn_6Sn_{6-x}In_x$ pseudo single crystal sample studied by ^{119}Sn Mössbauer spectroscopy under applied field [13]. It has been shown that when the Mn moment is made to rotate from the (0 0 1) plane to the [0 0 1] direction, the field of site Sn_{2e} decreased by −6.4 T and the fields of sites Sn_{2c} and Sn_{2d} increased by 1.9 and 2.1 T, respectively. This behaviour is linked to the expression of the total hyperfine field B_{hf} [13]:

$$\vec{B}_{hf} = A_p \sum_{i=1}^{6} \vec{u}_i(\vec{\mu}_i.\vec{u}_i) - \frac{A_p}{3}\sum_{i=1}^{6}\vec{u}_i + A_s\sum_{i=1}^{6}\vec{u}_i \qquad (3)$$

where A_p and A_s are the anisotropic and isotropic constants, $\vec{u}_i$ is the unit vector connecting each Sn atom to a specific Mn atom with moment $\vec{\mu}_i$. The last term is the isotropic contribution from

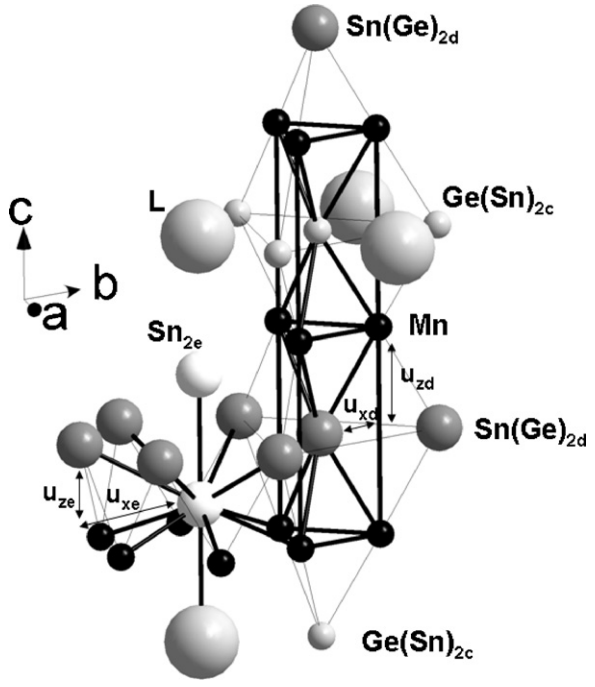

Fig. 7. Environment of the 2(c), 2(d) and 2(e) sites in the structure of $LMn_6Sn_4Ge_2$ (u_i are the components of the Mn–Sn unit bond [see Section 5.1]).

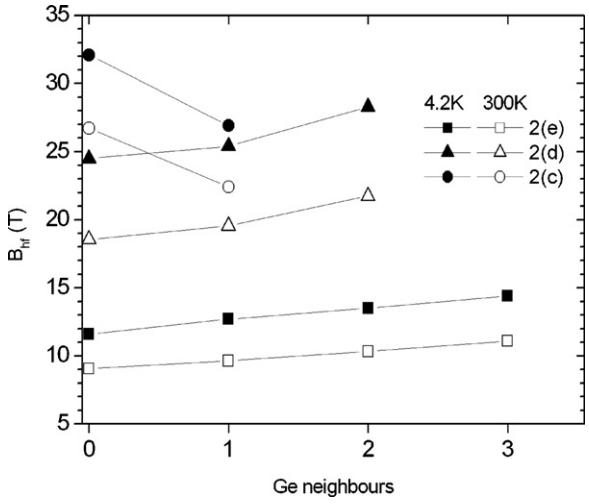

Fig. 8. Variation of the hyperfine field of the 2(c), 2(d) and 2(e) sub-sites as a function of the number of Ge neighbours.

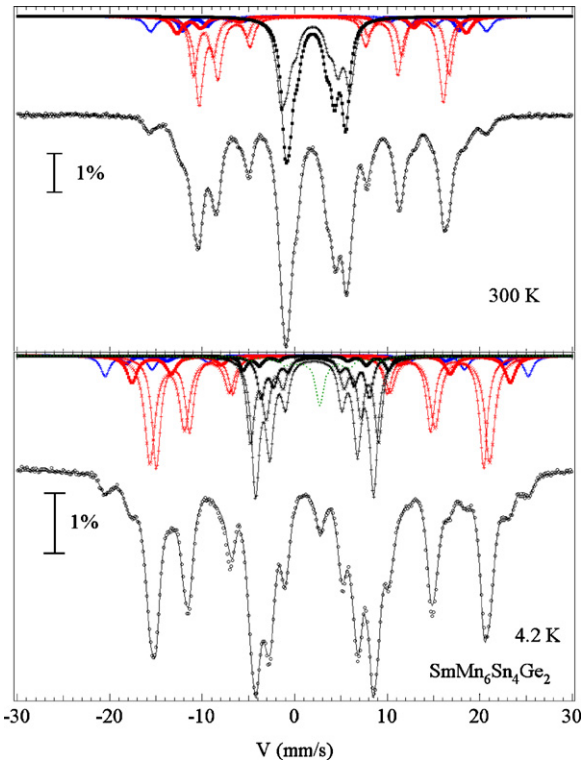

Fig. 9. Observed and calculated ^{119}Sn Mössbauer spectra of $SmMn_6Sn_4Ge_2$ at 300 and 4.2 K (the dotted line represents the impurities contribution).

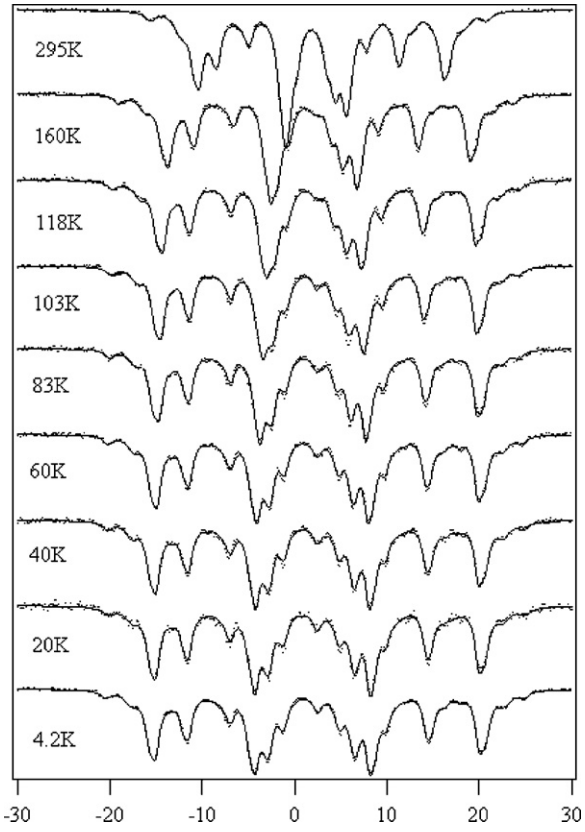

Fig. 10. ^{119}Sn Mössbauer spectra of $SmMn_6Sn_4Ge_2$ at various temperatures (the elemental tin peak is located around $v = 2.6$ mm/s).

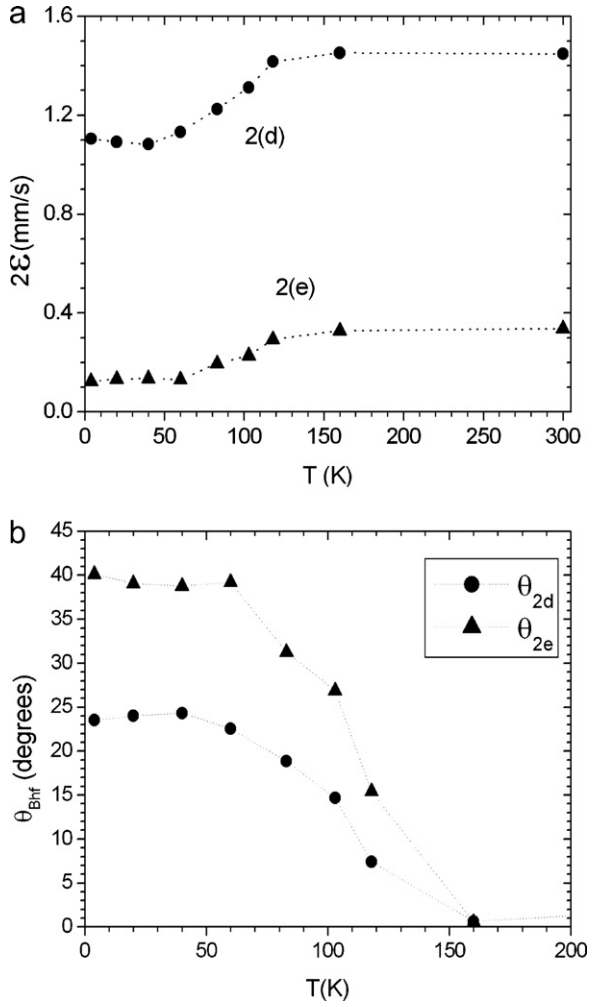

Fig. 11. (a) Thermal variation of the quadrupole splitting of the 2(d) and 2(e) sites of $SmMn_6Sn_4Ge_2$; (b) calculated θ angle according to Eq. (2) [see Section 5.1].

the Mn shells while the first two terms represent the anisotropic part of the transferred hyperfine field. It is worth noting that the magnitude and direction of the first term of Eq. (3) will depend on the relative direction between the moment and the Mn–Sn bonds. With moments rotating in the (x,z) plane, its vectorial components derived from Eq. (3) are:

$$\vec{B}_{\mathrm{ha}} = \left\|\mu\right\| A_{\mathrm{p}} \begin{pmatrix} 3u_x^2 \sin\theta \\ 0 \\ 6u_z^2 \cos\theta \end{pmatrix} \tag{4}$$

where u_x and u_y are the components of the Mn–Sn unit bond vector as depicted in Fig. 7 and θ the angle of the Mn moment with respect to the [0 0 1] direction. It may be observed that except for $\theta = 0$ and 90°, the direction of the anisotropic field is not parallel to the Mn moment and, in turn, to the direction of the isotropic field. It is also worth noting that, due to the relative $u_{x(e)}$ and $u_{y(e)}$ values related to the site Sn_{2e} (Fig. 7), the anisotropic field will be strongly reduced when the angle θ goes towards 0° while the $u_{x(d)}$ and $u_{y(d)}$ values related to the site Sn_{2c} and Sn_{2d} (Fig. 7) yield an increase of the corresponding anisotropic fields at the same time. These features agree with the behaviour of $YMn_6Sn_{6-x}In_x$ and allow a calculation of the angle dependent anisotropic contribution to the sites Sn_{2e} and Sn_{2d} (Table 6) [13]. In the following, we will estimate the angle dependent contribution (B_a) and remaining contribution (B_i) in $SmMn_6Sn_4Ge_2$ from the corresponding ratii in $YMn_6Sn_{6-x}In_x$ (Table 6) to schematically draw the field variations (magnitude and

Table 6
Observed hyperfine fields in $YMn_6(Sn,In)_6$ (B_{hf}), angle dependent anisotropic contribution ($B_a = B_{aniso}$) calculated via the field-induced reorientation process and difference ($B_i = B_{hf} - B_{aniso}$) [13]. The values of $SmMn_6Sn_4Ge_2$ are estimated from the characteristic ratio (*columns 6 and 7*) of $YMn_6(Sn,In)_6$ assuming similar constants of transferred field.

Sites	Orientation	B_{hf} (T)	B_{aniso} (T)(B_a)	$B_{hf} - B_{aniso}$ (T) (B_i)	B_a/B_{hf}	B_i/B_{hf}
$YMn_6(Sn,In)_6$						
2(d)	$\mu_{Mn} \perp [001]$	28.98	0.66	28.32	0.023	0.977
	$\mu_{Mn\ //} [001]$	31.08	2.76	28.32	0.089	0.911
2(e)	$\mu_{Mn} \perp [001]$	20.54	7.74	12.80	0.377	0.623
	$\mu_{Mn\ //} [001]$	14.14	1.34	12.80	0.095	0.905
$SmMn_6Sn_{\approx 4}Ge_{\approx 2}$						
2(d)	$\mu_{Mn\ //} [001]$	23.77	2.11	21.66	0.089	0.911
2(e)	$\mu_{Mn\ //} [001]$	6.83	0.65	6.18	0.095	0.905

direction) as a function of the angle ϕ_μ between the direction of the moments and the *c* axis.

Fig. 12 shows the geometric construction of the total transferred hyperfine field from the isotropic and anisotropic contributions for an angle ϕ_μ close to 25° and Fig. 13a shows the variation of the angle θ as a function of the angle of the moments (ϕ_μ). It is interesting to note that the angles of the total transferred field rather well mirror the experimental values deduced from the quadrupole splitting (Fig. 11). With the simplified starting values given in Table 6, the angle ϕ_μ ranges between 26 and 31° well accounting for the values deduced from magnetisation measurements.

As clearly observed in $YMn_6Sn_{6-x}In_x$, the hyperfine fields also vary at the moment re-orientation (Fig. 14). This is particularly sensitive for the site 2(e) since, in this case, the increase of the corresponding anisotropic field adds with the natural increase of the fields upon cooling. The calculation of the anisotropic and total field given in Fig. 13b displays an increase of B_{hf}(2e) by around 1 T and an equivalent decrease of B_{hf}(2d), values which are fully compatible with the observed variation (Fig. 14).

6. Discussion

Single-crystal magnetisation and ^{119}Sn Mössbauer spectroscopy measurements of $SmMn_6Sn_4Ge_2$ clearly evidence an easy-axis magnetocrystalline anisotropy between T_c and T_{SR} = 130 K and an easy-cone anisotropy below T_{SR}. This feature can be related to the previous magnetometric measurements undertaken on a polycrystalline sample which have shown a magnet-like behaviour at room temperature [1]. On another hand, ^{119}Sn Mössbauer spectroscopy studies, undertaken on the spherical Gd ion compounds, indicate an easy-plane anisotropy for $GdMn_6Sn_4Ge_2$ and $GdMn_6Sn_6$ and, therefore an easy-plane anisotropy of the Mn magnetic moment. This is in good agreement with the easy plane arrangement of the Mn moment deduced from the study of $LuMn_6Sn_4Ge_2$ [3]. The particular behaviour of $SmMn_6Sn_4Ge_2$ therefore accounts for the magnetocrystalline anisotropy of the Sm ion and may be compared to the results reported for isotypic $LMn_6Sn_4Ge_2$ compounds (L = Tb, Ho, Tm). According to neutron diffraction and ^{119}Sn Mössbauer spectroscopy experiments, these compounds display in-plane anisotropy at room temperature [3,5]. At low tempera-

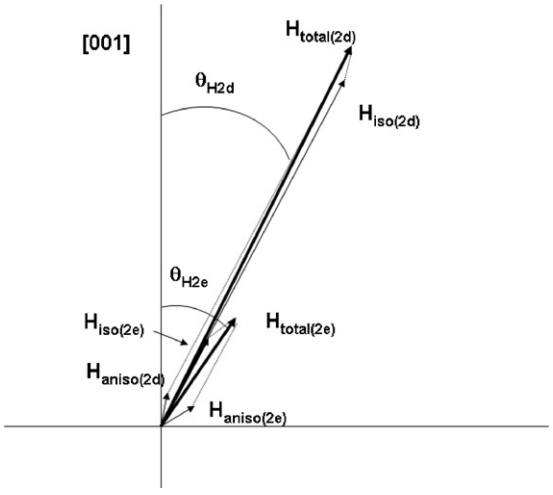

Fig. 12. Construction of the geometrical sum $\vec{B}_{hf} = \vec{B}_{iso} + \vec{B}_{aniso}$ for hyperfine fields of the 2(d) and 2(e) sites of $SmMn_6Sn_4Ge_2$ at 4.2 K.

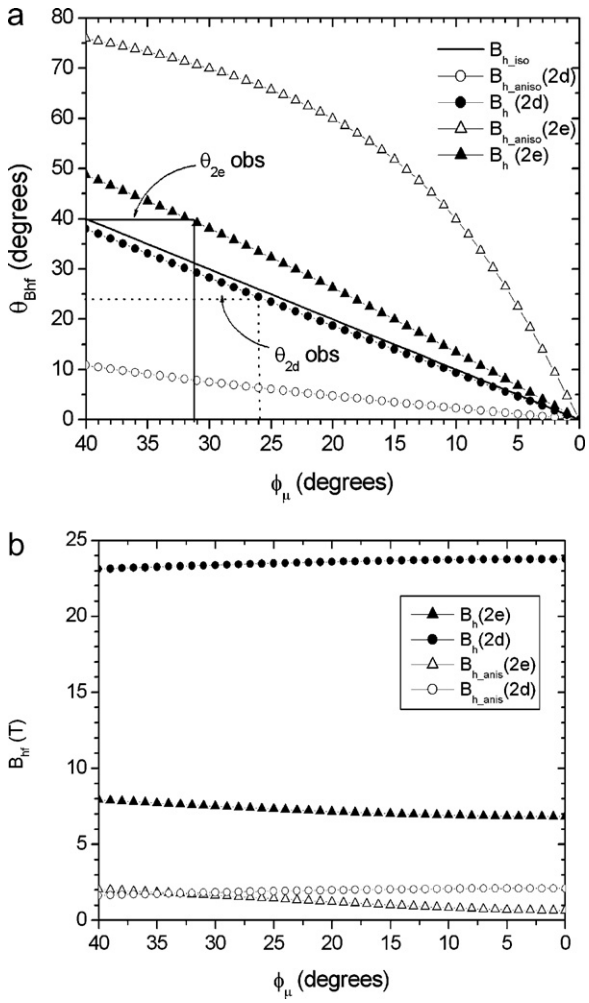

Fig. 13. (a) Calculated variation of the angle θ of isotropic, anisotropic and total hyperfine field of the 2(d) and 2(e) sites as a function of the angle of the moments; (b) calculated variation of the magnitude of the anisotropic and total hyperfine field of the 2(d) and 2(e) sites as a function of the angle of the moments.

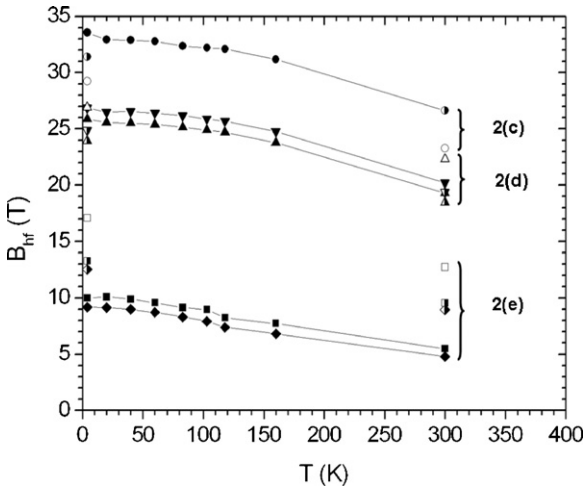

Fig. 14. Measured hyperfine fields of the main sub-sites 2(c) (circles), 2(d) (triangles) and 2(e) (squares) at various temperatures (open symbols: $GdMn_6Sn_6$; black symbols: $SmMn_6Sn_4Ge_2$; half-black symbols: $GdMn_6Sn_4Ge_2$).

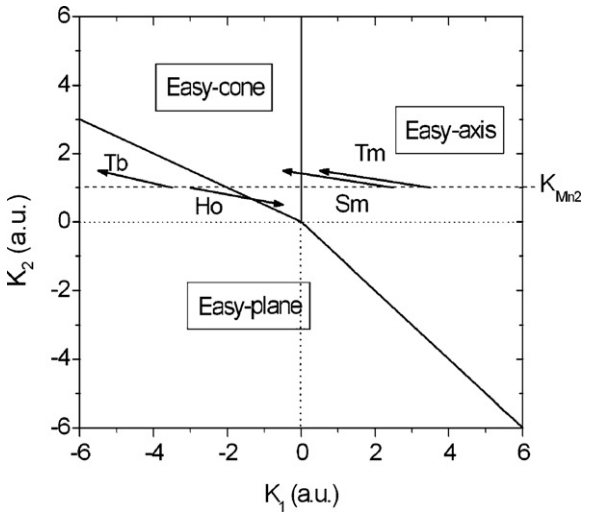

Fig. 15. Schematic stability diagram of the easy-axis, easy-plane and easy-cone anisotropy as a function of the K_1 and K_2 anisotropy constants for hexagonal $LMn_6Sn_4Ge_2$ compounds. The arrows indicate the possible variation of the constants at low temperature for positive A_4^0 crystal field parameter.

ture, the easy-plane anisotropy of $TbMn_6Sn_4Ge_2$ remains while $HoMn_6Sn_4Ge_2$ and $TmMn_6Sn_4Ge_2$ display easy-cone and easy-axis anisotropy, respectively [3,5]. Interestingly, the easy axis behaviour of $TmMn_6Sn_4Ge_2$ at low temperature and of $SmMn_6Sn_4Ge_2$ at RT on one hand, and the easy plane behaviour of the Tb compound on another hand are related to the positive sign of the α_j Steven's coefficient of the Sm and Tm ions and of the negative sign of α_j of the Tb ion. This suggests that the crystal field parameter A_2^0 is negative as observed in the $LMn_6Sn_4Ga_2$ compounds (L = Tb-Tm) previously studied [15–17]. As A_2^0 has changed its sign in LMn_6Sn_6 compounds with respect to $LMn_6Sn_4Ga_2$ compounds, it has been suggested that the different electronic structure of the Ga atom might be responsible of a change of the charge distribution around the L site. The present results and the data available for the other $LMn_6Sn_4Ge_2$ compounds (L = Tb, Ho, Tm), rather suggest that the smaller size of the Ge and Ga atoms could be responsible of this effect. The main effect of the small size of the Ge and Ga atoms is to induce a shortening of the L-Mn contacts. It is worth noting that, according to P. Schobinger-Papamantelos et al. [18,19], the LMn_6Ge_6 compounds (L = Er, Tm) are characterized by a skewed spiral structure with a relatively large angle between the normal to the spiral and the c axis (θ_s = 60 and 69°, respectively). This feature might also indicate an easy axis anisotropy of the Tm and Er ions in ternary germanides, namely in compounds characterized by rather short L-Mn contacts.

The moment reorientation from easy axis to easy cone is a transition of a new kind in this family of compounds. Neutron diffraction of $HoMn_6Sn_4Ge_2$ has evidenced a reorientation from easy plane to easy cone [3]. It probably involves particular values of the anisotropy constants. An exhaustive analysis of the stability of the cone anisotropy in hexagonal $Dy(Mn,Cr)_6Sn_6$ has been reported by Schobinger-Papamantelos et al. [20]. According to this report, the stability of the cone structure is related to the following conditions:

$$0 < -K_1 < 2K_2 \text{ and } K_1 < 0$$

where K_1 and K_2 are the total first- and second-order anisotropy constants. According to crystal field theory, the first and second-order anisotropy constants of the lanthanide K_1^L and K_2^L are given by:

$$K_1^L = -\frac{2}{3}\alpha_j\langle r^2\rangle A_2^0\langle O_2^0\rangle - 5\beta_j\langle r^4\rangle A_4^0\langle O_4^0\rangle$$
$$K_2^L = \frac{35}{8}\beta_j\langle r^4\rangle A_4^0\langle O_4^0\rangle$$

where A_2^0 and A_4^0 are the crystal field parameters which are not expected to vary much in isotypic compounds, $\langle O_2^0\rangle$ and $\langle O_4^0\rangle$ are the thermal averages of the second and fourth order Stevens operators which vary with temperature as high powers of the reduced lanthanide moment m_r (m_r^3 and m_r^{10}, respectively).

As the Stevens coefficients β_j of Ho and Sm have opposite sign, the low temperature condition $K_2 > 0$ cannot be fulfilled for both compounds without considering the contribution of a positive second-order anisotropy constant of the Mn sublattice in the total second order constant $K_2 = K_2^{Mn} + K_2^L$. In such a case and assuming a positive A_4^0 value, a possible scheme of the variation of the anisotropy constants K_1 and K_2 is proposed (Fig. 15). It shows that the strong increase of the $\langle O_4^0\rangle$ value at low temperature and its concomitant effect on the constants K_1^L and K_2^L allows the compounds $SmMn_6Sn_4Ge_2$ and $HoMn_6Sn_4Ge_2$ to both enter in the easy cone range. According to this schematic drawing, it seems that negative K_1^{Mn} and positive K_2^{Mn} anisotropy constants on one hand and negative A_2^0 and positive A_4^0 crystal field parameters, on the hand, might account for the anisotropy behaviour of the studied $LMn_6Sn_4Ge_2$ (L = Sm, Gd, Tb, Ho, Tm, Lu) series.

7. Conclusion

The study of $SmMn_6Sn_4Ge_2$ evidences a new behaviour never observed in other isotypic compounds. The anisotropy properties of the known $LMn_6Sn_4Ge_2$ might be related to particular values of anisotropy constants and crystal field parameters. It will be interesting to study the remaining compounds (L = Nd, Dy, Er) to check if their properties agree with these values. On another hand, this study has shown the useful information provided by the ^{119}Sn Mössbauer spectroscopy. It might be also of interest to investigate by this technique the other ternary or pseudo-ternary isotypic stannides.

References

[1] G. Venturini, J. Alloys Compd. 398 (2005) 42–47.
[2] F Weitzer, A. Leithe-Jasper, K. Hiebl, P. Rogl, Q.N. Qi, J. M.D. Coey, J. Appl. Phys. 73 (13) (1993) 8447.
[3] G. Venturini, B. Malaman, L.K. Perry, D.H. Ryan, J. Alloys Compd. 484 (2009) 59–68.
[4] B. Chafik El Idrissi, G. Venturini, B. Malaman, D. Fruchart, J. Less Comm. Met. 175 (1991) 143–154.
[5] L.K. Perry, RyanF D.H., G. Venturini, B. Malaman, J. Alloys Compd. 469 (2009) 34–41.
[6] J. Rodriguez-Carvajal, Physica B 192 (1993) 55.
[7] G. le Caër (private communication).
[8] C. Lefèvre, G. Venturini, B. Malaman, J. Alloys Compd. 354 (1–2) (2003) 47–53.
[9] T. Mazet, J. Tobola, B. Malaman, Eur. Phys. J. B33 (2003) 183.
[10] Y. Amako, T. Yamamoto, H. Nagai, Hyperfine Interact. 94 (1994) 1897.
[11] G. Venturini, B. Malaman, B. Ouladdiaf, J. Alloys Compd. 506 (2010) 36–45.
[12] G. Le Caër, B. Malaman, G. Venturini, I.B. Kim, Phys. Rev. B 26 (9) (1982) 5085–5096.
[13] L.K. Perry, D.H. Ryan, G. Venturini, Phys. Rev. B75 (2007) 144417.
[14] B. Malaman, G. Venturini, R. Welter, J.P. Sanchez, P. Vuillet, E. Ressouche, J. Magn. Magn. Mater. 202 (1999) 519–534.
[15] C. Lefèvre, G. Venturini, B. Malaman, J. Alloys Compd. 358 (2003) 29–35.
[16] L.K. Perry, D.H. Ryan, G. Venturini, J. Appl. Phys. 101 (2007), 09K504_1–4.
[17] C. Lefèvre, G. Venturini, B. Malaman, J. Alloys Compd. 346 (2002) 84–94.
[18] P. Schobinger-Papamantellos, G. André, J. Rodriguez-Carvajal, K.H.J. Buschow, J. Alloys Compd. 219 (1995) 176.
[19] P. Schobinger-Papamantellos, G. André, J. Rodriguez-Carvajal, J.H.V.J. Brabers, K.H.J. Buschow, J. Alloys Compd. 226 (1995) 113.
[20] P. Schobinger-Papamantellos, G. André, J. Rodriguez-Carvajal, H.G.M. Duijn, K.H.J. Buschow, J. Magn. Magn. Mater. 219 (2000) 22.